Identification of Important Locational, Physical and Economic Dimensions in Power System Transient Stability Margin Estimation

Robert I. Hamilton, *Student Member, IEEE*, Panagiotis N. Papadopoulos, *Member, IEEE*, Waqquas Bukhsh, *Senior Member, IEEE,* Keith Bell.

Abstract— **Increasing renewable generation can lead to significant spatial and temporal changes to the rotor angle stability boundary, such that critical contingencies may drastically change. Additionally, the inherent variability of renewables increases the number of operational scenarios that require stability assessment. This paper presents a methodology whereby a series of location-specific Decision Tree Regressors are trained, using power system variables to estimate the Critical Clearing Time (CCT) on a locational basis throughout a network. Permutation feature importance is used to reveal the most important power system variables for CCT estimation at each location (capturing aspects related to physical system characteristics, operational parameters as well as economic dispatch). Consequently, estimation of the duration and location of the critical fault can also be made – along with identification of important system variables that explicitly impact the critical fault. Results on the IEEE 39-bus network show accurate estimation of locational CCTs, with a mean absolute percentage error of 1.19% on average. Moreover, the mean absolute percentage error for the minimum CCT is 0.49%. An analysis of important power system variables is provided, demonstrating how the method can assist in the design of targeted locational interventions to improve the stability margin at specific locations.**

***Index Terms*--Critical clearing time, machine learning, power system stability, renewable generation, transient stability.**

I. Introduction

THE decarbonization of power systems is resulting in carbon intensive generators being replaced with intermittent renewable generation. This typically means a reduction in the number of traditional synchronous generators (SG) in favour of – often non-synchronous – renewable energy sources (RES). The consequent loss of SG attributes (upon which power systems have been built and operated for decades), and the complex highly non-linear dynamics associated with RES are proving challenging for maintaining system stability [1]. This has an impact on operability of the power system, in particular its dynamic response characteristics – especially transient stability [2]. In recognition of this, an IEEE taskforce revised the power system stability definition in 2020 [3]. Indeed, authors in [4] identify both improvements and deteriorations in the stability margin as a result of the connection of RES. Further to this, [5] demonstrates that there can be a shift in the critical fault due to the spatial, temporal and dynamic aspects introduced by RES, emphasising the growing need to closely monitor the stability of power systems and ensure critical contingency lists are updated as required. As the generation mix of power systems change, previous operational expertise may become outdated – driving the need for methods such as the one proposed in this paper.

Traditional approaches for transient stability assessment (TSA) are centred around two main approaches: time-domain simulation (TDS) and transient energy function (TEF) methods [6]. Whilst less time consuming and computationally burdensome than TDS, TEF methods are unable to replicate the level of detailed information available in TDS due to the use of simplified models. This is a key disadvantage in systems with high volumes of RES. The TDS approach (typically RMS) models the system dynamic components with differential-algebraic equations and solves them iteratively in time. TDS approaches suffer from the fact that simulation time is long, particularly for analysis of large systems. In addition to this, with the inclusion of RES, often widely dispersed across a network, the number of operational scenarios that needs to be studied in operational or investment planning timescales significantly increase. This further increases the computational burden of TDS, limiting their practical use. On the other hand, TEF methods derived from Lyapunov stability theory provide an analytical expression for the stability boundary that can be computed quickly but fail to capture key details such as the dynamic response from RES controllers. Researchers have overcome these limitations by coupling offline RMS TDS with online machine learning (ML), an approach this paper builds on through focusing on understanding locational aspects of transient stability and important parameters that affect them. Indeed, the ability to interrogate ML models is another key advantage of using ML over RMS TDS, where the high dimensionality of the problem is often too complex to understand.

Extensive research has gone into the application of various supervised ML techniques on transient stability in recent years. (Detailed reviews are presented in [7]–[10]). Among other methods, support vector machines (SVM) [11][12], artificial neural networks (ANN) [13][14] and decision trees (DT) [15][16], have been used. Trade-offs exist relating to factors such as training time, data pre-processing requirements, accuracy, and interpretability. Whilst the accuracy of estimation tends to increase in opaque black-box models (e.g. ANN), the white-box nature of DTs offers a high degree of transparency – enabling rule extraction, first discussed in [17].

This work was supported by EPSRC Centre for Doctoral Training in Future Power Networks and Smart Grids at the University of Strathclyde and Imperial College London EP/L015471/1 (R. I. Hamilton) and by the UKRI Future Leaders Fellowship MR/S034420/1 (P. N. Papadopoulos).

All results can be fully reproduced using the methods and data described in this paper and references provided.

The authors are with the Department of Electronic and Electrical Engineering at the University of Strathclyde, Glasgow, Scotland.

Although accuracy in the context of ML methods for TSA is very important, the particular focus of this paper is on interpretability. For a ML method to be useful for TSA, the objective of such a method should be to not only accurately determine the stability of an operating point, but also identify driving factors behind the outcome such that decisions on preventive or corrective control measures can be informed sufficiently quickly for them to be implemented without incurring undue risk in system operation. Indeed, the features selected to train a ML model significantly influence both the above. It is common for authors to use information collected after a fault happens to improve model accuracy [11], [18]–[21]. This is, however, at the expense of controllability since it allows only for corrective control actions as a last resort with very short activation times. Consequently, the use of pre-fault data in the transient stability estimation problem is advantageous in this regard [22]. With respect to interpretability, a method to identify important features relating to the small-signal stability problem is given in [23]. Similarly, the authors of [24] determine the degree of influence features have on the splitting property and estimation accuracy of the DT. Whilst the method considers increased output from RES, it seeks to predict SG rotor angle deviation and does not include features relating to displacement of SG by RES.

A key contribution of the methodology proposed by this paper is the identification of important power system features on a locational basis, providing a system wide perspective of features influencing the stability boundary, including the impact of RES. Whilst neither DT rule extraction or ML model interpretation are novel in and of themselves, the authors believe that the extraction of important features for stability *margin* estimation on a *locational* basis is a new contribution.

Indeed, another important consideration when designing a ML method for transient stability estimation is deciding what the model should predict (the so-called 'target'). The distinction between seeking to predict the stability status of a system or provide a quantitative prediction of the stability margin is also important to consider. Whilst classification methods in [25]–[30] offer insight into whether the operating point is stable or not, no information regarding the proximity of the operating point to the stability boundary is provided.

An improvement on this is through the calculation and use of the *critical clearing time* (CCT) metric [31], [32] as a measure of the stability margin. To calculate CCT using TDS the fault duration must be systematically varied, resulting in the requirement to run numerous simulations. This makes it significantly more computationally burdensome to calculate than the aforementioned metrics, with authors frequently citing this as a reason to not calculate CCT [8], [29]. Having said that, CCT is a detailed and informative means of assessing transient stability because the full dynamic response of the network is captured, revealing the proximity of an operational scenario to the stability boundary. Of particular interest is the *duration* and *location* of the short-circuit fault captured with the *minimum* CCT (CCT_{min}). This provides a metric describing the proximity of an operating point to the stability boundary – specifically relating to the minimum time for protection activation for the most critical fault and its location – the *critical fault location* (CFL). This further increases computational intensity since determination of CCT_{min} is dependent on calculating CCT at each fault location. Nonetheless CCT_{min} and CFL are important metrics that form the basis for critical contingency lists, which may be significantly impacted as more RES connects [5], [33].

Examples of CCT estimation through regression are more limited. However, some key examples can be found [34]–[37]. As is the case in most of the literature, these studies do not consider all fault locations, meaning that only a small section of the stability boundary is considered. Therefore, no further analysis around variations in CCT_{min} and CFL are provided. In addition, the impact of connection of RES is not considered. This is a significant drawback since connection of RES may result in a reduction in CCT_{min} and a change in the CFL depending on the state of RES operation at the time of the fault, as demonstrated in [5]. Often, a limited number of fault locations is assessed by system operators (SO) and planners based on experience and judgment. However, when faced with a wide variety of hitherto unfamiliar system conditions in addition to the changing dynamic behavior due to RES connection, it becomes important to assess a much larger number of fault locations and form contingency lists appropriately. This paper seeks to meet this need through a system-wide location-based ML approach to (a) estimate the transient stability margin and (b) provide details of the important power system variables that influence the stability boundary. Such information can be useful to SOs and system planners for identifying critical locations and taking action to improve transient stability throughout the network, both in operational and planning timescales. The key novel contributions from this paper include:

1) a methodology capable of the identification of the most important power system variables that impact the stability margin (specifically the critical clearing time (CCT) determined using RMS-TDS and thus maintaining detailed estimation) using Permutation Feature Importance (PFI),

2) the inclusion of features related to physical system characteristics as well as economic dispatch (dictating generator dispatch), allowing for identification of complex trends impacting transient stability at different locations of a system. This approach can assist SOs and system planners in the design of targeted interventions,

3) accurate estimation of the stability margin on a locational basis throughout the network without the need to perform TDS online. Location-specific representations of the stability boundary in parameter space are generated. The locational and graphical nature of the proposed method enables identification of changes to the critical fault duration and location. Results can inform updates to credible contingency lists by being used as a fast-screening tool as well as inform the generation of rules for operational and planning decisions.

II. Methodology

The methodology developed in this paper is summarised in Fig. 1, consisting of off-line and on-line processes (black shaded and red unshaded respectively). A transient stability database (TSDb) consisting of power system variables and CCTs (described in Section II. B.) for each of the n fault locations across z operational scenarios is generated in the offline phase using RMS TDS. The TSDb is then used to construct n DT regressor models for local CCT estimation (Section II. C). Permutation Feature Importance (PFI) is subsequently applied to each location-specific DT model to identify the most important features for CCT estimation per location (Section II. D). Threshold values for the important features from decision nodes in the DT models are extracted

and a feature space representation of the stability boundary with threshold values is established on a locational basis (Section II. E). Since RES can have a significant impact on the duration and location of the critical fault [5], specifically estimating CCT_{min} and CFL is important. Two methods are proposed for doing so.

- *Method A*: CCT_{min} is estimated by identifying the minimum CCT from each of the *n* locational DT model estimates and the CFL is taken as that location.
- *Method B*: A single DT regression model is constructed specifically to estimate CCT_{min}. In addition, a DT classifier is constructed to estimate CFL.

Both method A and B require the same computational effort for RMS TDS, however method B explicitly trains trees to estimate CCT_{min} and CFL. Consequently, method B offers additional details relating to the important features to CCT_{min} specifically compared to method A. Therefore, method B supplements method A by providing these additional details.

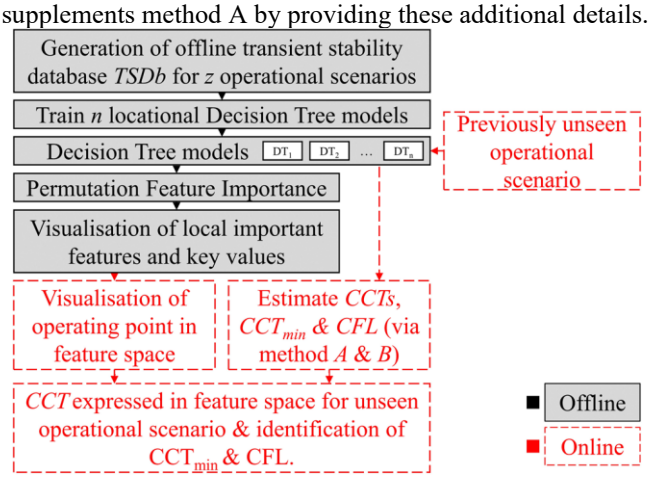

Fig. 1. Proposed methodology for stability margin estimation and identification of important locational features.

In the online phase, previously unseen operational scenarios can be evaluated using the locational stability boundary representation (based on important features and threshold values extracted from DT models), providing an informative and intuitive means of assessing the factors responsible for shaping the stability boundary.

A. Operational scenarios and the AC Optimal Power Flow

An operational scenario of a power system is defined as a particular realization of demand, wholesale electricity markets preference for generation dispatch, and a network state. In this paper, the AC optimal power flow (OPF) problem is used as a proxy to model the preference of a wholesale electricity system for dispatching generation that satisfies operational constraints. As a result, the OPF determines the initial operating conditions and consequently has a significant impact on transient stability. The objective function for an AC OPF [38] is to find a steady state operating point that minimises the cost of generation while satisfying operating constraints and meeting demand. The AC OPF used here that in is MATPOWER [38] where each generator's cost is modelled by a standard polynomial cost function:

$$Cost = c_0 + c_1 P_e + c_2 P_e^2 \ \$/hr \quad (1)$$

where P_e is the electrical power output and c_0, c_1 and c_2 are cost coefficient values. The Locational Marginal Price (LMP) of electricity at a location (busbar), λ_n, is defined as the least cost to meet the next increment of demand at that location. Diverging LMPs between busbars are indicative of active power flow constraint(s), reflected in the associated Karush Kuhn Tucker (KKT) multiplier(s). Since a KTT only becomes non-zero once a constraint is active; additional information about the system, such as congested parts of the network, is provided [39]. In this paper OPF variables are included in the TSDb for this reason. The main advantage of such an approach being not necessarily to improve the predictive performance of the model, but identify key tendencies and interventions that affect system stability.

B. Transient Stability Database Creation

The fundamental concept behind ML methods for TSA is to train a model offline, capable of identifying the relationship between power system variables (features, *X*) and the transient stability of a system (target, *Y*), using a number of simulated responses. Timely decision making is critical in system operation, especially in circumstances in which the systems state is changing rapidly. Once the relationship between the features and the target is established, previously unseen scenarios can be approximated with reduced computational effort online, quick stability assessment is important.

It should also be noted that feature selection for ML methods is important regarding estimation accuracy and interpretability of results. As previously mentioned, the use of pre-fault data is advantageous over fault-on data since the former offers more time to take corrective actions. With the above points in mind, the methodology proposed here deliberately does not limit the features that can be included in the TSDb, however features gathered from measurement devices (i.e. *pre-fault operational* variables) should be considered mandatory. This includes demand level, generator output, resulting power flows, network voltages and angles. These operational variables are fundamental in determining transient stability [31] and are frequently included in relevant literature (e.g. [24]). Additional features can be included to supplement the above variables, depending on the application and the insights desired. Any redundant features are eliminated using RFE-CV during the model training stages (Section II. C). In Section III and IV in this paper, a case study is presented where additional features relating to physical characteristics of the system (generator ratings, inertia, active and reactive power limits and elements of the network admittance matrix) as well as economic dispatch (total cost, LMPs and KKTs) are included. Details of these features (and the motivation for inclusion) are presented in Section III. D in Table I and impact on TSA discussed. While we propose the use of physical and economic dispatch related features in this paper to derive useful insights, the exact features are defined in detail in Section III to highlight the fact that the method offers flexibility in the choice of features. An interesting avenue for future research would be the inclusion of control variables in the TSDb in order to assess and understand their impact on dynamics (e.g. changes to RES controller settings).

The target for each locational DT model is the CCT for the corresponding network location since this quantifies the proximity of an operating point to the stability boundary. The CCT for a particular fault is determined through iteratively increasing the fault duration by 0.01 sec until loss-of-synchronism (LOS) of a SG is detected using RMS TDS. As such, all control behaviour of all the generators – including RES – is captured in the CCT metric. A limit of π degrees on

the rotor angle deviation between any two machines for identifying LOS is used, as follows:

$$\Delta\delta_{ab} = \delta_a - \delta_b > \pi \quad (2)$$

where δ_a and δ_b are the rotor angles of SGs a and b. An upper limit for CCT estimation of 1.4 sec is imposed, beyond which the system is considered far from the stability boundary. For a given operational scenario, the shortest CCT out of all the fault locations, n, analysed is the CCT_{min} (3) and its location – the CFL. This results in identification of both the duration and location of the critical fault.

$$CCT_{min} = \min\{CCT_1, CCT_2 \dots CCT_n\} \quad (3)$$

In this paper, the CCTs for faults on busbars are calculated, under the assumption that the shortest CCT for a transmission line connecting two busbars would be at either of the two busbars. Ultimately, the degree of granularity required in the locational estimation of CCT and CCT_{min} is depends on engineering judgement. However, since the computational effort is focused during the offline stages of this method, it is recommended that as many faults as possible are assessed since [5], [33] demonstrate that the critical contingency can significantly vary as RES connects.

C. Decision Tree Regression and Algorithm

A decision tree (DT) is constructed for each busbar on the network, seeking to estimate CCT at the corresponding location. DTs are constructed using the principle of recursively splitting training samples into smaller subsets (with similar target variables) in a top-down manner until a stopping criterion is met [40]. They are particularly useful when there are non-linear complex relationships between features and the target – which is the case for the transient stability problem with increasing penetration of RES. A simple DT structure is provided in Figure 2.

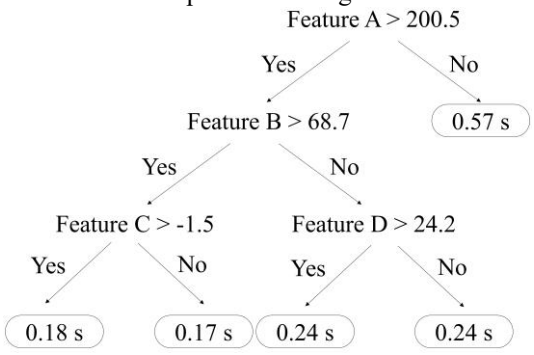

Fig. 2. Simple DT structure

Specifically, for training vectors $x_j \in X$, with p features where $j = 1, \dots, p$ and target vector Y, the DT recursively partitions the feature space, grouping data with similar target values. Let Q_m represent the data at node m be represented by with N_m samples. For each candidate split $\theta = (j, t_m)$ consisting of a feature j and threshold value t_m, data is partitioned into left and right subsets ((4) and (5) respectively) [41].

$$Q_m^{left}(\theta) = \{(x, Y) | x_j \leq t_m\} \quad (4)$$

$$Q_m^{right}(\theta) = Q_m / Q_m^{left}(\theta) \quad (5)$$

The ability of DTs to determine the relationship between large numbers of features with non-linear relationships and the CCT with no data pre-processing is a significant advantage over other methods [7]. Moreover, the intuitive representation of how the features impact the outcome and transparency of the decision-making process lends itself well to assisting in developing an understanding of the complexities of the stability boundary. For example, the threshold value t_m for feature j can be extracted from the candidate split θ, for important features (Section II. D.) providing numerical limits for important features. Threshold values for candidate splits lower down the DT provide a higher degree of confidence in prediction accuracy (e.g. a prediction difference of ±0.01 sec), whilst higher splits highlight higher level trends in CCT (e.g. ±0.10 sec).

1) Decision Tree Regression Algorithm: The Classification and Regression Trees (CART) algorithm from scikit-learn package in Python [41] is used. The usefulness of the algorithm for regression in power systems is demonstrated in [42]. The algorithm seeks to minimize a cost metric for future splits. This paper uses the mean absolute percentage error (MAPE), which is appropriate for CCT estimation since it accounts for the relative size of errors, described mathematically:

$$MAPE(y, \hat{y}) = 1/N \sum_{i=1}^{N} |y_i - \hat{y}_i| / max(\epsilon, |y_i|) \quad (6)$$

where y_i is the actual value, $\hat{y_i}$ is the estimated value, N is the number of data points, i is the observation and ϵ is an arbitrary small positive number (to avoid undefined results). The output will be between 0 and 1, where a score closer to 0 indicates a more accurate model.

2) Feature Elimination during Training: Removal of features that have little predictive power avoids overfitting and improves model accuracy. This paper uses Recursive Feature Elimination with Cross Validation (RFE-CV) [41] to do so. First, the TSDb is partitioned into training (80 %) and testing (20 %). Subsequently, a DT model is repeatedly trained using different combinations of features to find the set of features that result in the highest model score. The wrapper-type algorithm selects the optimal number of features for a model by recursively removing features, until the set of features that results in the best model score is identified (starting with the entire TSDb). The model is scored using repeated stratified k-fold cross-validation [41].

D. Permutation Feature Importance (PFI)

Permutation Feature Importance (PFI) is a process to determine most influential features from a ML model [43]. In this paper, PFI is applied to each location-specific DT model to rank features based on their importance for estimation of CCT at that location. This is done by evaluating the change in DT model score when individual features are permutated, breaking the relationship between the feature and the true outcome. The reference score (using MAPE (6)) of the model M for the dataset X with target vector Y is computed based on error measure $L(Y, M)$. For k repeats in $k = 1, \dots, K$, each feature $j = 1, \dots, p$ in the dataset is randomly shuffled to generate a corrupted version of the data $\tilde{X}_{k,j}$. The score ($score_{k,j}$) of model M on the corrupted data is then computed and the importance i_j of each feature determined by (7). This results in location-specific ranking of features based on feature importance for local CCT estimation.

$$i_j = score - 1/k \sum_{k=1}^{K} score_{k,j} \quad (7)$$

E. Feature-Space Stability Boundary Representation

A visual representation of the stability boundary at each location can be generated through combining important feature list (Section II. D) and corresponding threshold values

(Section II. C). This is possible due to the white-box nature of DTs. Previously unseen operational scenarios can be superimposed onto the stability boundary representation, offering operational context with respect to the stability margin on a locational basis (relative to important features and key threshold values). For stability boundary visualisation on a cartesian coordinate system, the three top-ranked important features at each location are of interest. The CCT at each location can be added as a fourth dimension to the color axis. Threshold values t_m (4) for each important feature are extracted from the corresponding DT model and added as flat surfaces to the plot, highlighting key stability turning points are in the feature space. In this paper the uppermost candidate split is taken, but additional threshold values could be extracted from subsequent candidate splits in the DT depending on the level of detail required.

F. Additional Performance Metrics for Testing

For the final stage of analysis using the testing portion of the TSDb, four additional performance metrics are used. The coefficient of determination (R^2) and the square root of the mean square of all errors (RMSE) are given by:

$$R^2 = 1 - \sum_i^N (y_i - \hat{y}_i)^2 / \sum_i^N (y_i - \bar{y}_i)^2 \quad (8)$$

$$RMSE = \sqrt{\sum_{i=1}^N (y_i - \hat{y}_i)^2 / N} \quad (9)$$

where N is the number of data points, i is the observation, y_i is the actual value, $\hat{y_i}$ is the estimate and $\bar{y_i}$ the mean of all observations. Additional metrics relating to the maximum errors are also defined since an under-estimate of the CCT, may result in an overly cautious dispatch. This may be good from a system security perspective but may result in increased costs of system operation. Conversely, an over-estimate may provide a false sense of security, potentially resulting in a higher risk of instability. For this reason, the maximum over-estimation and under-estimation absolute errors (MOE and MUE) are determined.

$$MOE = max\,(y_i - \hat{y}_i) \quad (10)$$

$$MUE = min\,(y_i - \hat{y}_i) \quad (11)$$

In addition, the MOE and MUE for the most critical faults (defined here as cases where the actual CCT < 0.30 sec) is also determined, since a large error in a more critical fault may have more severe consequences.

III. Test Network and Case Study Details

The method is demonstrated on an adapted version of the IEEE 39-bus test network (Fig. 3). The RMS TDS simulations are carried out in DIgSILENT PowerFactory [44] and the AC OPF is solved in MATPOWER [45]. A set of operational scenarios, designed to represent how the generation connected to the system may change as a result of planning or operational decisions (i.e. closure of SG plant and the opening of windfarms, which may be as a consequence of government policy), is defined in Section III. C.

A. Network Overview and Operational Scenarios

The network nominal voltage is 345 kV at a nominal frequency of 60 Hz. The total active power demand of the network is 6097.1 MW, modelled as balanced three-phase constant impedance loads. SGs (G01-G10) are represented by four-winding 6th order models, with full details regarding given in [45]. The network topology remains unchanged throughout the studies (i.e. no line tripping or network reconfigurations are studied).

International Electrotechnical Commission (IEC) Type-4A wind turbines [46] are used to model wind generation in the RMS framework. Therefore, the dynamic characteristics of wind and its controller, including the fault-ride-through (FRT) capabilities (i.e. reduction in active power and injection of reactive power), on the networks dynamic response is captured. The controller operates at unity power factor pre-fault. This may vary between systems and will impact reactive power dispatch and thus transient stability. A windfarm is treated as an aggregate of individual 2 MW turbines connected in parallel, each with its own transformer. Three generation areas are defined with different colors (Fig. 3) for the purpose of connection of SG and disconnection of RES in Section II. C.

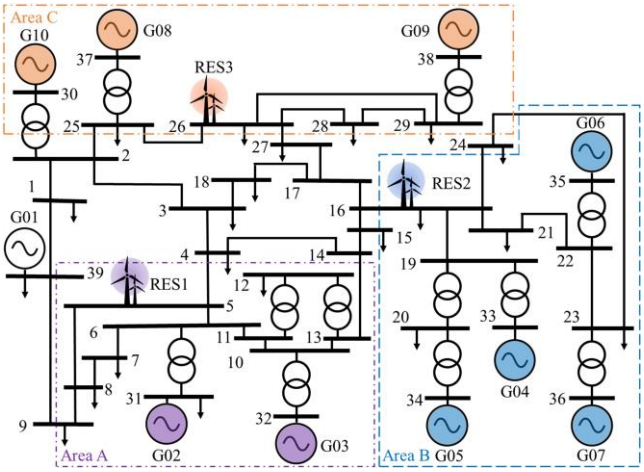

Fig. 3. Adapted version of the IEEE 39-bus network.

B. Generator Dispatch via AC OPF

A full AC OPF is implemented in MATPOWER to establish generator dispatch, where cost coefficients representative of different types of generation are taken from [47] are allocated to generators as specified in [48]. RES is considered to have zero marginal cost and therefore are dispatched at full active power output. The merit order of generators is determined through the polynomial cost function (1). SG active and reactive power dispatch limits are 0.2 to 0.85 p.u. and -0.25 to 0.5 p.u respectively (based on machine MVA rating). Network voltages limits are 0.94 to 1.06 p.u. of nominal voltage.

C. Generation of Operational Scenarios

The range of operational scenarios considered are designed to represent the various operational scenarios that may arise due to displacement of conventional SG (as fossil-fuel used less frequently or retired) by RES (as windfarms are constructed). Three factors are varied to generate the operational scenarios: SG connected, RES connected and system demand. Specifically, one SG is displaced by RES connecting in the same generating area at a time. Each SG is considered an equivalent generator consisting of four equal-sized units, therefore each SG can be disconnected in four stages (12). The new MVA rating of $SG_{MVA,new}$ is based on the number of remaining generating units, u (where u = 1, 2, 3, 4 and is rated to $SG_{MVA,old}$). Should the potential network conditions or operational scenarios of interest change over time, it may be necessary to retrain the ML models with an updated set of scenarios.

The capacity of RES connecting to the network is scaled in a similar, inverse, manner (13). However, an additional penetration scaling factor, s (where s = 0, -0.05, 0.05 in this paper), is included to decouple any proportional relationship

between decreasing SG MVA rating (and subsequent reduction in inertia) and increasing RES MVA rating. In addition, a scaling factor, r (where r = 1, 1.4 in this paper, representing high and very high renewable penetration respectively), is applied to account for high-RES output scenarios. RES is rounded up to the nearest even value since each RES unit is rated at 2 MVA. Scenarios with no displacement are also considered. Total system demand is varied uniformly throughout the network from 0.6 to 1.025 p.u., based on the initial power flow of the network (given in [44]), in 0.025 p.u. increments.

$$SG_{MVA,new} = u\,(SG_{MVA,old}/4) \quad (12)$$

$$RES_{MVA} = r\left(((5-u)\,SG_{MVA,old}/4) + s\left(SG_{MVA,old}\right)\right) \quad (13)$$

3906 operational scenarios are designed based on 18 demand levels, 36 SG disconnection stages (9 SGs, each disconnected in 4 stages) and 6 RES levels. The RES penetration in relation to SG capacity for generating areas A, B and C ranges from 0% to 131%, 59% and 54% respectively This is equivalent to varying the instantaneous RES penetration from 0 to 47% of total active power generation. This results in 3888 displacement scenarios, plus 18 scenarios with no displacement. From these 3906 operational scenarios, 144 (that is 3.7 %) do not result in a successful convergence of the OPF solution. For the successfully converged scenarios (3762, that is 96.3%) RMS TDS are executed using DIgSILENT PowerFactory, for all fault locations. Fault locations considered in this case study are three-phase-to-ground busbar faults excluding both the LV terminal busbars for all SGs (9 busbars) and all RES points of common coupling (3 busbars), resulting in a total of 27 fault locations. It should be noted that the generation of scenarios to be included in the training database is important to reflect realistic possible operating conditions of the system. For this reason, we generate the operational scenarios taking into consideration a realistic approach for various system loading and renewable generation conditions, as well as the impact of economic dispatch. In addition, the achieved accuracy can be used as indication that further training might be required.

D. Feature Selection for Transient Stability Assessment

As outlined in the methodology (Section II. B.), the inclusion of *pre-fault operational* variables (relating to generator dispatch, resulting network voltages and power flows) should always be included in the TSDb. Additional features can be added to the TSDb, for a particular application where additional insights may be required. Including additional targeted features may offer some additional predictive power and/or enhance understanding of factors impacting the stability boundary.

This paper is particularly focused on the impact of decommissioning of SG and rapid connection of RES. As such, *system variables* relating to the physical attributes of the network and its generators are included as features in the TSDb. In particular, parameters relating to the amount of SG connected and the location of RES with respect to SG have been shown to significantly impact the stability boundary such that the critical fault may change [5]. Therefore, variables relating to SG machine size (MVA rating and operational limits), inertia of the installed generation in various network areas are included. In addition parameters relating to the proximity of SG to RES are included as variables since the spatial impact of displacement is demonstrated in [5], where the FRT behavior of RES is shown to impact the angular stability of nearby SG. As such, key elements of the network admittance matrix relating to the proximity of SG to RES are included.

Generator dispatch is the consequence of physical constraints and preference of a wholesale electricity market that satisfies operational constraints at least cost given what is available at the time (using OPF as a proxy). Indeed, the link between generator dispatch and transient stability is the basis of the transient stability constrained OPF problem [49]. Due to this inherent link between the market, generator dispatch and consequent transient stability margin: variables from the OPF solution are included. For example, recent fluctuations in European gas prices [50] may change the merit order of generators. Motivation for including these is two-fold: to determine whether they enhance the predictive power of the method and what additional insight(s) they can provide (discussed in more detail in Section V).

A particular output of the OPF problem that is of interest is LMP of electricity at a location (busbar), denoted by λ_n, and KTMs. Since LMPs account for the physical limitations of generators, the network, demand and cost (1-4), they may offer some predictive power. Moreover, LMPs are traditionally used to identify areas with insufficient (or surplus) generation. Generation in such areas may be running at high active power output due to a constraint, leading these machines closer to the stability boundary. Finally, since KKTs only become non-zero once the constraint is active, KKTs can provide additional insight and a systematic means of identifying the active constraint. Therefore, they could be used to inform planning decisions e.g. identify bottlenecks/constraints that impact the stability boundary which could be used to identify areas where reinforcements may be required. The cost of these reinforcements can be compared to the cost of re-dispatching to form the basis of a cost-benefit analysis. For a system with k generating areas, v SG units, w RES units, l loads and n busbars, this results in 1061 features that are included in the TSDb in Table I.

TABLE I
FEATURE SELECTION BY CATEGORY

Mandatory	Additional	
Pre-fault Operational	System	Market
$P_{d,l}$ $Q_{d,l}$ $SG_{P,v}$ $SG_{Q,v}$ $RES_{P,w}$ $RES_{Q,w}$ $v_{bus,n}$ $v_{bus,\delta,n}$ $P_{from,n}$ $P_{to,n}$ $Q_{from,n}$ $Q_{to,n}$	$SG_{MVA,v}$ $SG_{MVA,k,total}$ $SG_{MVA,total}$ $SG_{H,v}$ $SG_{H,k,total}$ $SG_{H,total}$ $SG_{xd',v}$ $RES_{MVA,w}$ $RES_{MVA,total}$ $SG_{P,max,v}$ $SG_{P,min,v}$ $SG_{Q,max,v}$ $SG_{Q,min,v}$ $Y_{bus,key}$	λ_n *KKT Cost/hr*

The inclusion of system, market and operational variables means that insights relating to how the economic dispatch of available generation (that may vary depending on the extent to which RES connects and SG disconnect) and resulting power flows impact the stability boundary. This can assist in not only operational but also planning timescales.

E. Computational Details

The RMS TDS (performed in DIgSILENT PowerFactory) and ML training were conducted on an Intel® Core™ i7-6700 CPU @3.40GHz with 16 GB installed RAM. For each RMS-TDS, an average of 40 seconds are required to calculate the CCT. Using this PC specification, a single DT can be trained in approximately 60 minutes. Both the RMS TDS for construction of the TSDb and the ML algorithm training is conducted offline when more time is generally available, making this less important. The time critical stage is the estimation of the stability margin, which can be achieved in approximately 0.2 seconds (a 200-fold reduction in computational time), for a single tree using the pre-trained ML algorithms. This is significantly shorter than calculating CCT using automated RMS TDS.

IV. Results

The following section details key results and findings from implementing the proposed methodology on the IEEE 39-bus network for the case study previously described.

A. Locational CCT Estimation

As outlined in Section II B, the CCT for a short-circuit fault provides a metric that captures the proximity of the operating point to the stability boundary. Since we use RMS TDS, the full dynamic response of the network is captured in the CCT metric. Table III outlines the performance for each locational DT model for the 752 test cases (the testing portion is 20 % of the TSDb). Results show a high degree of accuracy for all DT models, with MAPE averaging 1.19 % (ranging 0.03–2.20 % at B12 and B18 respectively). As previously described MAPE (6) is used as the cost metric during DT model training since it accounts for the relative size of errors, which is particularly important when estimating CCT. In addition, the results show strong performance in R^2 values averaging 0.9859 (ranging 0.9555–0.9975 at B27 and B21/B22) and RMSE averaging 0.0223 sec (ranging 0.0030–0.0648 sec at B19 and B07).

In many cases the MOE is significant, averaging 0.24 sec across all DT models (ranging 0.02–0.78 sec at B19/B20 and B07). However large overestimates of short a CCT is of even greater significance. For these most critical faults (taken as < 0.30 sec), the average MOE reduces to 0.03 sec (ranging 0.00–0.14 sec at B06 and B13). Fig. 4 shows the actual versus estimated CCT, with MOE and MUE metrics capturing outliers that are significantly reduced when considering only short CCTs (since MAPE is consistently small). This highlights the efficacy of using MAPE as the cost metric, when estimating CCT. Should these outliers be of concern, the DT cost metric can be changed to include a square in the error term (e.g. R^2, given in (8) of RMSE in (9)).

TABLE II
Performance Metrics for Different Tree-Based ML Algorithms

Target	DT	RF
MAPE (%)	1.19	1.41
R^2	0.9859	0.9898
RMSE (sec)	0.0223	0.0164
MOE (sec)	0.24	0.16
MUE (sec)	-0.18	-0.13
MOE < 0.3 sec (sec)	0.0331	0.0300
MUE < 0.3 sec (sec)	-0.0144	-0.0138

Another means of performance enhancement is to use a more complex ML algorithm. One such tree-based algorithm is Random Forrest (RF) [43], which is an ensemble of DTs. Whilst estimation accuracy improves (Table II), this is at the expense of diminished insights. While PFI can still be applied to RF (and indeed more complex black-box algorithms e.g. Deep Neural Networks), the rule extraction described in Section II. E is only possible with DTs. This tension is well documented in ML literature [51]. The degree of accuracy achieved using DTs is only negligibly worse than RF while the inherent interpretability of DT models due to their transparent nature is offers the possibility to extract rules as described in Section II. E.

TABLE III
Performance Metrics for Selection of Location-Based DTs

Location	B04	B24	B27	B13	B17
MAPE (%)	1.41	1.34	2.10	0.95	1.80
R^2	0.9911	0.9933	0.9555	0.9960	0.9852
RMSE (sec)	0.0354	0.0122	0.0645	0.0111	0.0194
MOE (sec)	0.60	0.11	0.53	0.14	0.19
MUE (sec)	-0.14	-0.07	-0.47	-0.04	-0.08
MOE < 0.3 sec (sec)	n/a	0.01	0.01	0.14	0.01
MUE < 0.3 sec (sec)	n/a	-0.02	-0.02	-0.01	0.00
Location	B39	B23	B20	B22	B19
MAPE (%)	0.80	0.69	0.38	0.77	0.32
R^2	0.9869	0.9974	0.9772	0.9975	0.9816
RMSE (sec)	0.0081	0.0049	0.0031	0.0054	0.0030
MOE (sec)	0.05	0.03	0.02	0.03	0.02
MUE (sec)	-0.07	-0.03	-0.01	-0.03	-0.02
MOE < 0.3 sec (sec)	n/a	0.03	0.02	0.03	0.02
MUE < 0.3 sec (sec)	n/a	-0.01	-0.01	-0.03	-0.02
Location	B06	B10	B29	B25	B02
MAPE (%)	1.41	0.81	0.84	1.06	1.51
R^2	0.9891	0.9971	0.9792	0.9804	0.9711
RMSE (sec)	0.0294	0.0067	0.0138	0.0121	0.0195
MOE (sec)	0.34	0.07	0.07	0.14	0.24
MUE (sec)	-0.18	-0.02	-0.23	-0.20	-0.11
MOE < 0.3 sec (sec)	0.00	0.07	0.01	0.02	0.10
MUE < 0.3 sec (sec)	0.00	-0.02	-0.01	-0.02	-0.01

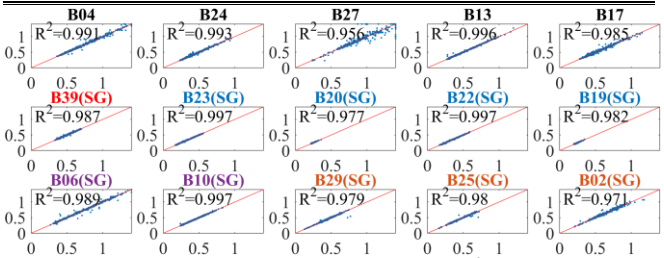

Fig. 4. Actual vs. estimated CCT at each busbar with R^2 value given.

B. Identification of CCT_{min} and CFL

A key highlight of the proposed method is the ability to identify both the CCT_{min} and CFL for a previously unseen operational scenario. In doing so, amendments to credible contingency lists can be provided as required as the system conditions or characteristics change. The performance and advantages of both methods proposed in Section II. are compared below. The actual versus estimate for CCT_{min} for each method is given in Fig. 5 and the performance metrics in Table IV. Both methods achieve a similar degree of accuracy in estimation of both CCT_{min} and CFL, with method A are slightly outperforming method B (Table IV). In terms of CFL estimation, method A correctly locates the CFL in 96.5 % of test cases (726/752). For method B - where a new DT classifier is trained to estimate CFL – the CFL is correctly located in 96.3 % of test cases (724/752). Despite this, the performance difference for CCT_{min} estimation between method A and B can is marginal. However, the key advantage of method B over A is that important features for CCT_{min} estimation can be determined. The advantages of doing so are discussed in Section IV. D.

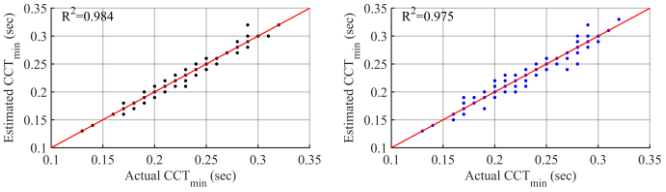

Fig. 5. Actual versus estimated CCT_{min}, for method A (left) and B (right).

TABLE IV
PERFORMANCE METRICS FOR EACH CCT_{MIN} ESTIMATION METHOD

Target	Method A CCT_{min}	Method B CCT_{min}
MAPE (%)	0.49	0.65
R^2	0.9838	0.9745
RMSE (sec)	0.0035	0.0044
MOE (sec)	0.03	0.03
MUE (sec)	-0.02	-0.03
MOE < 0.3 sec (sec)	0.03	0.03
MUE < 0.3 sec (sec)	-0.02	-0.03

C. Identification of changes in CCT_{min} and switch in CFL

The efficacy of the method to identify variations in local CCTs that ultimately result in a variation in CCT_{min} and switch in CFL in the context of increased RES is illustrated using two example operational scenarios. Both scenarios have the same level of demand (0.9 p.u.). Scenario A has 280 MVA of RES3 connected to bus 26 and no disconnection of SG. In scenario B, three of the four generating units that make up G08 are disconnected, and RES3 is rated at 932 MVA. Therefore, between scenario A and B RES accounts for 10% and 43% or the total generating capacity in area C respectively.

Between scenario A and B, the CCT at B23 improves from 0.21 to 0.24 sec but CCT at B25 deteriorates significantly from 0.42 to 0.19 sec, as shown in Table V. These two opposing locational trends ultimately lead to a deterioration in CCT_{min} from 0.21 to 0.19 sec and a switch in CFL from B23 (Area B) to B25 (Area A) – i.e. the CFL shifts from one location to another. This example shows good accuracy, with each locational CCT being accurately predicted. In addition to this, CCT_{min} and CFL are correctly identified for both scenarios by method A. However, method B misidentifies the CFL for scenario B. The capability of the method to identify such instances where the critical fault unpredictably changes (in both duration and location) due to displacement is of value to system planners and operators. Identifying such behaviors could inform the definition of credible contingency lists.

TABLE V
SCENARIOS SHOWING SWITCH IN CFL DUE TO INCREASED DISPLACEMENT

Operational Scenario details			Method A estimates				Method B estimates		Actual RMS TDS results			
Scenario	RES3	G08	CCT B23	CCT B25	CCT_{min}	CFL	CCT_{min}	CFL	CCT B23	CCT B25	CCT_{min}	CFL
A (red circle)	280	700	0.21	0.42	0.21	B23	0.21	B23	0.21	0.42	0.21	B23
B (red square)	932	175	0.24	0.19	0.19	B25	0.19	B23	0.24	0.19	0.19	B25

D. Stability Boundary Representation in Feature Space

A location-specific feature-space representation of the stability boundary can be generated for each location, as outlined in Section II. E. This provides insights into how variations in local important features between operational scenarios may impact local CCT (and ultimately the CCT_{min} and CFL). The feature-space representation of the stability boundary for B23 and B25 is given in Fig. 6 and Fig. 7 respectively. For each feature, the uppermost threshold values t_m (4) is indicated by the transparent colored surface (red indicating the most important feature and green the least). These values can be extracted due to the white-box nature of DTs. Scenario A and B (large red circle and square respectively) are superimposed. Such a representation is generated for all locations but have been omitted from this paper due to space constraints (however the top-three important features for a selection of locations are detailed in Table VI). In doing so identification of trends impacting transient stability can be identified, as outlined in the paper contributions.

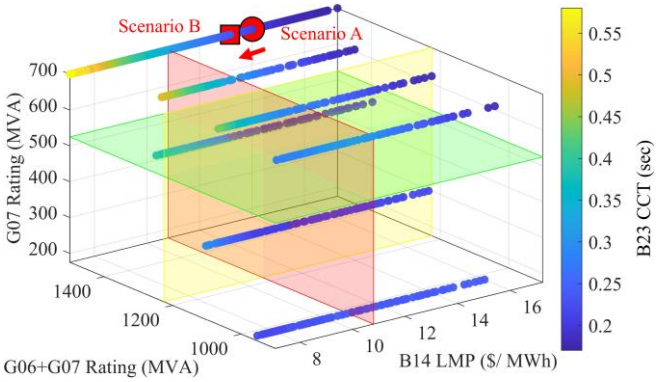

Fig. 6. Important feature space representation of B23 stability boundary showing scenario A (large red circle) and Scenario B (large red square) with B23 CCT (sec) on color axis.

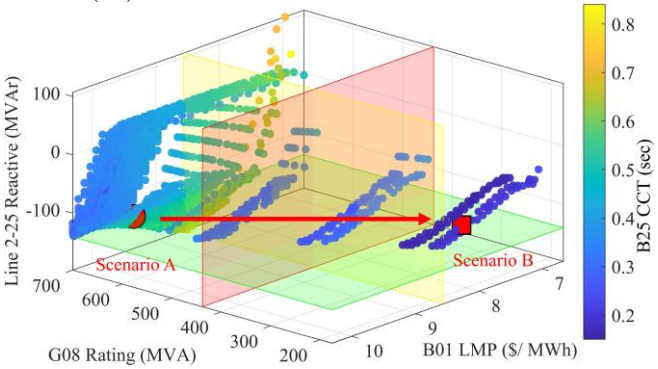

Fig. 7. Important feature space representation of B25 stability boundary showing scenario A (large red circle) and Scenario B (large red square) with B25 CCT (sec) on color axis.

A system planner or operator may reasonably conclude – through inspection of B23 stability boundary representation (Fig. 6.) – that to avoid such a significant reduction in the CCT at B23, disconnection of G06 or G07 should be avoided. Similarly, G08 should remain connected as far as possible if the stability of the system following a B25 fault is of concern.

Whilst this is informative of locational trends, the overall stability boundary can be assessed through analysis of Fig. 8, which shows important features for CCT_{min} estimation using method B. These are identified as B03 LMP, the combined MVA rating of G08 and G09, and the dispatch of G05. The feature space is partitioned using the uppermost threshold value of each important feature from the DT, giving an indication of critical values for each important feature where CCT_{min} worsens. For example, when B03 LMP > 14.93 $/MWh (the threshold value for B03 LMP, described by the red surface in Fig. 8), CCT_{min} is on average 23 % higher than if LMP < 14.93 $/MWh. Similarly, if G08 and G09 combined MVA rating > 1187.5 MVA, CCT_{min} is 25 % higher than if less than this threshold. Finally, if line 20-34 active power flow < 236.34 MW, the average CCT_{min} is 15 % higher. When all three feature thresholds are crossed, CCT_{min} is on average 29 % lower, providing situational awareness of CCT_{min} with respect to these important features. Combining this with the locational stability boundary information provided by the DT models distributed throughout the network provides a network-wide view of the stability boundary. For example, disconnection of G06 and G07 worsens the stability for B23 faults but is preferable in terms of overall stability to disconnect of G08.

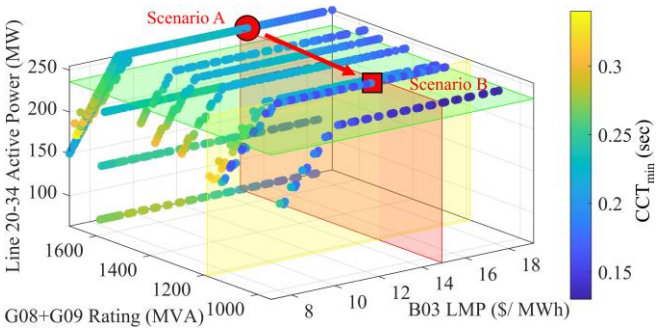

Fig. 8. CCT_{min} (sec) on the color axis expressed in top-three feature space with DT threshold values for each added, partitioning feature space and highlighting operational zones that result in longer or shorter CCT_{min}.

E. Local stability boundary improvements using important features

The identification of important features on a locational basis enables locational manipulation of power system variables (directly or indirectly) to improve CCT at that location. For example, the most important feature for CCT estimation at B17 is identified as the KKT for line 2-3 power flow (Table VI), coinciding with a divergence of LMP at B03. The KKT for line 2-3 power flow only becomes active once the constraint is active (i.e. the desired power transfer on the line would be equal to or greater than the line capacity). This bottleneck in the network and the extent to which it impacts the final OPF solution is only identified because OPF features were included in the TSDb.

To test the efficacy of the method in identifying features that do indeed impact the stability boundary, the capacity of line 2-3 was increased. This is achieved by adding an additional identical circuit, re-running the OPF and running TSD to determine CCT at B17 across all operational scenarios. Fig. 9 shows the minimum CCT for a B17 fault increasing from 0.28 to 0.36 sec and the median CCT increasing from 0.49 to 0.58 sec. In improving the stability boundary at this location, the likelihood of CCT_{min} being at this location is reduced, although it should be noted that other locations may be adversely impacted. This highlights the ability for the method to identify important features on a locational basis, enabling testing and development of targeted interventions – as outlined in the paper contributions. Similar analysis can be conducted to assess the impact of other important features at different locations.

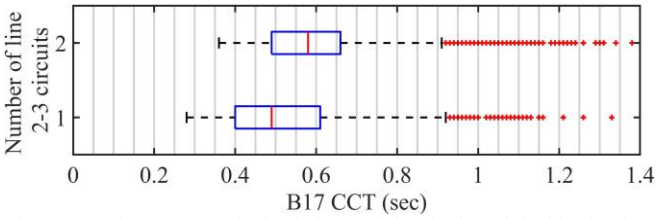

Fig. 9. Actual B17 CCT (obtained via TDS) for single and double circuit at line 2-3.

V. Discussion

Features included in the TSDb for the case study presented above included market, pre-fault operational and system variables to assist in identification of how operational decisions and displacement patterns impact stability. Since the market (OPF is used as a proxy in this paper) determines the generator dispatch which subsequently impacts the stability boundary, OPF variables were included as features in the TSDb. The inclusion of such variables is valuable if the consequence is to (a) enhance prediction accuracy and/or (b) offer additional insight(s) into the stability boundary. Upon repeating the method above for the same operational scenarios, excluding the OPF features, the average MAPE across all DT models remains unchanged (1.19 %). Since there is no additional performance benefit from including OPF features, a discussion around the potential benefits in terms of interpretability is given below.

TABLE VI
Three Top-Ranked Features from PFI for Selection of Locations

	B04	B24	B27	B13	B17
1	B04 LMP	Line 12-11 MVAr	B03 LMP	B04 LMP	KKT Line 2-3
2	G03 x_d'	Area B MVAs	G09 x_d'	G03 x_d'	Line 19-20 MVAr
3	B13 LMP	B14 LMP	Line 5-6 MW	B11 LMP	B03 LMP
	B39	B23	B20	B22	B19
1	Line 1-39 MW	B14 LMP	G05 MW set	B14 LMP	Line 20-34 MW
2	B01 LMP	G06 + G07 MVA	B20 LMP	G06 + G07 MVA	RES2-G04
3	Line 2-25 MW	G07 MVA	B14 Vang	Line 23-36 MW	G04 + G06 MVAs
	B06	B10	B29	B25	B02
1	B20 LMP	G02 x_d'	G09 x_d'	G08 MVA	G08 + G10 MVA
2	G03 MVA	B04 LMP	B27 LMP	B01 LMP	RES3-G09
3	KKT V B01	B11 LMP	Total Cost	Line 2-25 MVAr	B25 LMP

OPF features such as LMP encapsulate multiple features in a single value, as described in (1-4). Moreover, KKT can identify constraints/ bottlenecks, offering additional insights. The LMP at a busbar represents the cost associated with meeting the next unit of demand at that busbar. In a system with comparatively priced generation (as in this paper), a high LMP is associated with a lack of generation in an area and is often used as a signal to indicate where there is insufficient generation capacity. Conversely, a low LMP is a signal for demand to connect. It follows that LMP in the context of transient stability is an indicator for the loading of nearby SGs with respect to RES output and demand level. This provides a means of identifying network locations that may have poor transient stability margin (although other factors also come into play). This may be an indicator for requiring some preventative measure, such as operationally limiting the output of SGs in that area or technological solutions such as braking resistor installations in areas with consistently high LMPs. KKTs give the cost associated with an active constraint. A divergence of LMPs at different locations indicates an active constraint in the system, meaning that the least-cost dispatch cannot be achieved due to some constraint. Such a constraint can be identified through the other KKTs (e.g. KKT for maximum power output of a generator etc) – where a non-zero value for a KKT indicates an active constraint. This points towards the root the causes of divergence of LMPs and may assist in design of measures to improve transient stability (e.g. network reinforcement).

In addition to this, the OPF solution provides a means of assessing the cost implications of moving to a new – more transiently stable – operating point. For example, the cost of moving from scenario B to A in Section IV. C. would be 6,858 $/hr, for a 0.02 sec improvement in CCT_{min}. Similarly, the cost of a network reinforcement can be compared. This could form the basis of a cost-benefit analysis for assessing technological vs operational stability improvement methods. A focus for future work could develop a new optimization

problem with the aim of maximizing CCT_{min} and minimizing cost with respect to the important system features.

VI. Conclusions

Increasing volumes of renewable energy resources (RES) in power systems can lead to considerable changes to the transient stability margin, such that critical contingency lists may become outdated. In addition, the number of potential operational scenarios requiring assessment increases – making the use of time-domain simulations impractical. Therefore, there exists a need to assess the transient stability of new operational scenarios quickly and accurately, with sufficient detail to identify variations in critical faults. Identification of the underlying factors that impact the stability boundary on a locational basis is crucial for the design and development of stability enhancement measures.

This paper proposes the combined use of location-specific machine-learning (ML) approach with model inspection technique – permutation feature importance (PFI) – to identify locational important variables. A series of location-based decision tree (DT) regressors are trained to estimate the critical clearing time (CCT) at each network location and important features to the prediction of CCT for each location are identified. In addition, two methods for estimation of the duration and location of the critical fault (CCT_{min} and Critical Fault Location - CFL) are proposed and compared. Method A utilizes all locational DT models, seeking to identify the minimum. The second, Method B, builds additional DT models to specifically estimate CCT_{min} and CFL.

In the case-study provided, pre-fault operational variables are supplemented with market and system variables (physical system characteristics) for model training. This enables the impact of the economic dispatch of available generators and displacement patterns to be uncovered. As such, analysis of both operational and planning decisions can be made. Results using the IEEE 39-bus network show a high degree of accuracy for all DT models, with the mean absolute percentage error (MAPE) averaging 1.19% across all DT models. Important parameters for the estimation of CCT at each location are extracted using PFI. A system-wide stability boundary representation is established and threshold values from DTs extracted (a key motivation for using DTs over potentially more accurate, but less transparent black-box models), highlighting turning points in the parameter-space representation of the stability boundary per location.

Estimation of CCT_{min} is accurate for both proposed methods. Method A achieves a MAPE of 0.49 %. The CFL is also correctly identified in 96.5 % of cases. Method B achieves a MAPE of 0.65 %. The CFL is also correctly identified in 96.3 % of cases. A case study is provided highlighting the method's ability to track CCT_{min} in feature space as network conditions change, as well as monitoring any locational shift in CFL. In doing so, an understanding of the underlying important power system features responsible for changes to the stability margin is revealed. Credible contingency lists can be updated accordingly.

The locational nature of the method means that an understanding of the parameters impacting the entire stability boundary are uncovered. As demonstrated in a case study, this can be used to target interventions at a particular location. In addition to this since the critical fault is also accurately estimated and important parameters identified, interventions can also be targeted at improving this.

References

[1] J. O'Sullivan, A. Rogers, D. Flynn, P. Smith, A. Mullane, and M. O'Malley, "Studying the maximum instantaneous non-synchronous generation in an island system—Frequency stability challenges in Ireland," *IEEE Trans. Power Syst.*, vol. 29, no. 6, pp. 2943–2951, 2014.

[2] P. Kundur *et al.*, "Definition and classification of power system stability," *IEEE Trans. Power Syst.*, vol. 19, no. 2, pp. 1387–1401, 2004.

[3] N. Hatziargyriou *et al.*, "Stability definitions and characterization of dynamic behavior in systems with high penetration of power electronic interfaced technologies," 2020.

[4] D. Gautam, V. Vittal, and T. Harbour, "Impact of increased penetration of DFIG-based wind turbine generators on transient and small signal stability of power systems," vol. 24, no. 3, pp. 1426–1434, 2009, doi: 10.1109/TPWRS.2009.2021234.

[5] R. I. Hamilton, P. N. Papadopoulos, and K. Bell, "An investigation into spatial and temporal aspects of transient stability in power systems with increasing renewable generation," vol. 115, p. 105486, Feb. 2020, Accessed: Jan. 25, 2021. [Online]. Available: http://www.sciencedirect.com/science/article/pii/S0142061519316758.

[6] H. D. Chiang, *Direct methods for stability analysis of electric power systems: theoretical foundation, BCU methodologies, and applications*. John Wiley & Sons, 2011.

[7] O. A. Alimi, K. Ouahada, and A. M. Abu-Mahfouz, "A review of machine learning approaches to power system security and stability," *IEEE Access*, vol. 8, pp. 113512–113531, 2020.

[8] A. R. Sobbouhi and A. Vahedi, "Transient stability prediction of power system; a review on methods, classification and considerations," *Electr. Power Syst. Res.*, vol. 190, p. 106853, 2021.

[9] S. You *et al.*, "A Review on Artificial Intelligence for Grid Stability Assessment," in *2020 IEEE International Conference on Communications, Control, and Computing Technologies for Smart Grids (SmartGridComm)*, Nov. 2020, pp. 1–6, doi: 10.1109/SmartGridComm47815.2020.9302990.

[10] J. Sohoni and S. K. Joshi, "A Survey on Transient Stability Studies for Electrical Power Systems," in *2018 Clemson University Power Systems Conference (PSC)*, 2018, pp. 1–8, doi: 10.1109/PSC.2018.8664072.

[11] A. D. Rajapakse, F. Gomez, K. Nanayakkara, P. A. Crossley, and V. V Terzija, "Rotor angle instability prediction using post-disturbance voltage trajectories," *IEEE Trans. Power Syst.*, vol. 25, no. 2, pp. 947–956, 2009.

[12] F. R. Gomez, A. D. Rajapakse, U. D. Annakkage, and I. T. Fernando, "Support Vector Machine-Based Algorithm for Post-Fault Transient Stability Status Prediction Using Synchronized Measurements," *IEEE Trans. Power Syst.*, vol. 26, no. 3, pp. 1474–1483, 2011, doi: 10.1109/TPWRS.2010.2082575.

[13] N. Amjady and S. F. Majedi, "Transient stability prediction by a hybrid intelligent system," *IEEE Trans. Power Syst.*, vol. 22, no. 3, pp. 1275–1283, 2007.

[14] F. Hashiesh, H. E. Mostafa, A.-R. Khatib, I. Helal, and M. M. Mansour, "An intelligent wide area synchrophasor based system for predicting and mitigating transient instabilities," *IEEE Trans. Smart Grid*, vol. 3, no. 2, pp. 645–652, 2012.

[15] M. He, J. Zhang, and V. Vittal, "Robust online dynamic security assessment using adaptive ensemble decision-tree learning," *IEEE Trans. Power Syst.*, vol. 28, no. 4, pp. 4089–4098, 2013.

[16] T. Guo and J. V Milanović, "Probabilistic framework for assessing the accuracy of data mining tool for online prediction of transient stability," *IEEE Trans. Power Syst.*, vol. 29, no. 1, pp. 377–385, 2013.

[17] L. Wehenkel and M. Pavella, "Decision tree approach to power systems security assessment," *Int. J. Electr. Power Energy Syst.*, vol. 15, no. 1, pp. 13–36, 1993.

[18] L. Zhu, D. J. Hill, and C. Lu, "Hierarchical Deep Learning Machine for Power System Online Transient Stability Prediction," *IEEE Trans. Power Syst.*, vol. 35, no. 3, pp. 2399–2411, May 2020, doi: 10.1109/TPWRS.2019.2957377.

[19] M. Rahmatian, W. G. Dunford, A. Palizban, and A. Moshref, "Transient stability assessment of power systems through wide-area monitoring system," in *2015 IEEE Power & Energy Society General Meeting*, 2015, pp. 1–5.

[20] T. Liu, Y. Liu, L. Xu, J. Liu, J. Mitra, and Y. Tian, "Non-parametric statistics-based predictor enabling online transient stability assessment," *IET Gener. Transm. Distrib.*, vol. 12, no. 21, pp. 5761–5769, 2018.

[21] M. Rahmatian, Y. C. Chen, A. Palizban, A. Moshref, and W. G. Dunford, "Transient stability assessment via decision trees and multivariate adaptive regression splines," *Electr. power Syst. Res.*, vol. 142, pp. 320–328, 2017.

[22] Y. Zhang, Y. Xu, Z. Y. Dong, Z. Xu, and K. P. Wong, "Intelligent Early Warning of Power System Dynamic Insecurity Risk: Toward Optimal Accuracy-Earliness Tradeoff," *IEEE Trans. Ind. Informatics*, vol. 13, no. 5, pp. 2544–2554, Oct. 2017, doi: 10.1109/TII.2017.2676879.

[23] S. Asvapoositkul and R. Preece, "Decision tree-based prediction model for small signal stability and generation-rescheduling preventive

control," *Electr. Power Syst. Res.*, vol. 196, p. 107200, 2021.
[24] F. Gonzalez-Longatt *et al.*, "MVMO-Based Identification of Key Input Variables and Design of Decision Trees for Transient Stability Assessment in Power Systems With High Penetration Levels of Wind Power," *Front. Energy Res. | www.frontiersin.org*, vol. 8, p. 41, 2020, doi: 10.3389/fenrg.2020.00041.
[25] L. Wehenkel, T. Van Cutsem, and M. Ribbens-Pavella, "An artificial intelligence framework for online transient stability assessment of power systems," *IEEE Trans. Power Syst.*, vol. 4, no. 2, pp. 789–800, 1989.
[26] L. Wehenkel, M. Pavella, E. Euxibie, and B. Heilbronn, "Decision tree based transient stability method a case study," *IEEE Trans. Power Syst.*, vol. 9, no. 1, pp. 459–469, 1994.
[27] T. Amraee and S. Ranjbar, "Transient instability prediction using decision tree technique," *IEEE Trans. power Syst.*, vol. 28, no. 3, pp. 3028–3037, 2013.
[28] Y. Chen, S. M. Mazhari, C. Y. Chung, S. O. Faried, and B. C. Pal, "Rotor Angle Stability Prediction of Power Systems With High Wind Power Penetration Using a Stability Index Vector," *IEEE Trans. Power Syst.*, vol. 35, no. 6, pp. 4632–4643, Nov. 2020, doi: 10.1109/TPWRS.2020.2989725.
[29] B. Li, J. Wu, L. Hao, M. Shao, R. Zhang, and W. Zhao, "Anti-Jitter and Refined Power System Transient Stability Assessment Based on Long-Short Term Memory Network," *IEEE Access*, vol. 8, pp. 35231–35244, 2020.
[30] I. Kamwa, S. R. Samantaray, and G. Joos, "Development of rule-based classifiers for rapid stability assessment of wide-area post-disturbance records," *IEEE Trans. Power Syst.*, vol. 24, no. 1, pp. 258–270, 2009.
[31] P. Kundur, N. N. J. Balu, and M. G. M. Lauby, *Power system stability and control*, vol. 7. McGraw-hill New York, 1994.
[32] J. Machowski, J. W. Bialek, and J. R. Bumby, *Power System Dynamics: Stability and Control*. New York: Wiley, 2008.
[33] M. Ma, W. Jie, Z. Wang, and M. W. Khan, "Global Geometric Structure of the Transient Stability Regions of Power Systems," *IEEE Trans. Power Syst.*, p. 1, May 2019, doi: 10.1109/tpwrs.2019.2919442.
[34] J. Lv, M. Pawlak, and U. D. Annakkage, "Prediction of the Transient Stability Boundary Based on Nonparametric Additive Modeling," *IEEE Trans. Power Syst.*, vol. 32, no. 6, pp. 4362–4369, 2017.
[35] W. Phootrakornchai and S. Jiriwibhakorn, "Online critical clearing time estimation using an adaptive neuro-fuzzy inference system (ANFIS)," *Int. J. Electr. Power Energy Syst.*, vol. 73, pp. 170–181, 2015.
[36] Z. Chen, X. Han, C. Fan, H. Zhang, and C. Liu, "Prediction of Critical Clearing Time for Transient Stability Based on Ensemble Extreme Learning Machine Regression Model," in *2019 IEEE Innovative Smart Grid Technologies-Asia (ISGT Asia)*, 2019, pp. 3601–3606.
[37] X. Liu, Y. Min, L. Chen, X. Zhang, and C. Feng, "Data-driven transient stability assessment based on kernel regression and distance metric learning," *J. Mod. Power Syst. Clean Energy*, 2020.
[38] R. D. Zimmerman, C. E. Murillo-Sánchez, and R. J. Thomas, "MATPOWER: Steady-state operations, planning, and analysis tools for power systems research and education," *IEEE Trans. power Syst.*, vol. 26, no. 1, pp. 12–19, 2010.
[39] A. J. Conejo, E. Castillo, R. Mínguez, and F. Milano, "Locational marginal price sensitivities," *IEEE Trans. Power Syst.*, vol. 20, no. 4, pp. 2026–2033, 2005.
[40] L. Breiman, J. Friedman, R. Olshen, and C. Stone, *Classification and Regression Trees*. 1984.
[41] F. Pedregosa *et al.*, "Scikit-learn: Machine learning in Python," *J. Mach. Learn. Res.*, vol. 12, pp. 2825–2830, 2011.
[42] R. Diao, V. Vittal, and N. Logic, "Design of a real-time security assessment tool for situational awareness enhancement in modern power systems," *IEEE Trans. Power Syst.*, vol. 25, no. 2, pp. 957–965, 2009.
[43] L. Breiman, "Random forests," *Mach. Learn.*, vol. 45, no. 1, pp. 5–32, 2001.
[44] DIgSILENT GmbH, "DIgSILENT PowerFactory User Manual," 2019.
[45] M. A. Pai, "Energy function analysis for power system stability," 1989.
[46] P. Sorensen, B. Andresen, J. Fortmann, and P. Pourbeik, "Modular structure of wind turbine models in IEC 61400-27-1," 2013, pp. 1–5, doi: 10.1109/PESMG.2013.6672279.
[47] R. Preece, *A probabilistic approach to improving the stability of meshed power networks with embedded HVDC lines*. The University of Manchester (United Kingdom), 2013.
[48] R. Hamilton, "GitHub MATPOWER IEEE 39-bus network case building script," *GitHub*, 2021. https://github.com/RobertIHamilton/MatPower_IEEE39Bus.git (accessed May 07, 2021).
[49] Y. Xu, Z. Y. Dong, Z. Xu, R. Zhang, and K. P. Wong, "Power system transient stability-constrained optimal power flow: A comprehensive review," in *2012 IEEE Power and Energy Society General Meeting*, 2012, pp. 1–7, doi: 10.1109/PESGM.2012.6344753.
[50] T. Wilson and N. Hume, "European gas prices shoot to new high as energy crunch worsens," Dec. 21, 2021.
[51] I. Bratko, "Machine Learning: Between Accuracy and Interpretability," in *Learning, Networks and Statistics*, 1997, pp. 163–177.

BIOGRAPHIES

Robert Hamilton was awarded a Master's degree in Electrical and Electronic Engineering (MEng) from the University of Strathclyde in 2016, where he graduated with Distinction. He since joined the EPSRC Centre for Doctoral Training in Future Power Networks and Smart Grids at the University of Strathclyde specializing in power system stability and dynamics for power systems with high penetrations of renewable generation. Particular research interests relate to the development of machine learning techniques to address the complexity of system dynamic behavior.

Panagiotis N. Papadopoulos (S'05-M'14) received the Dipl. Eng. and Ph.D. degrees from the Department of Electrical and Computer Engineering at the Aristotle University of Thessaloniki, in 2007 and 2014, respectively. Currently, he is a Senior Lecturer and a UKRI Future Leaders Fellow in the Department of Electronic and Electrical Engineering at the University of Strathclyde. His research interests are in power system stability and dynamics, focusing on tackling the increasing uncertainty and complexity in the system dynamic behaviour.

Waqquas Bukhsh is a Research Fellow at the Department of Electronics and Electrical Engineering, University of Strathclyde. He has a B.Sc. degree in mathematics from COMSATS University, and a Ph.D. degree in operational research from the University of Edinburgh. His research interests are in data analytics, optimisation problems and their applications to energy systems.

Keith Bell holds the ScottishPower Chair in Smart Grids at the University of Strathclyde and is a Co-Director of the UK Energy Research Centre (UKERC), a Fellow of the Royal Society of Edinburgh, a member of the UK's Climate Change Committee and a Chartered Engineer. Before joining Strathclyde, he worked as a system development planner in the electricity supply industry in England and as a researcher in Bath, Naples and Manchester. He has provided advice on power systems issues to parties including the Scottish Government, the Office of Gas and Electricity Markets (Ofgem) in Britain, the UK Government and the Government of Ireland and is active in CIGRE.